Science Advances
AAAS

Supplementary Materials for

Structure of the rabies virus glycoprotein trimer bound to a prefusion-specific neutralizing antibody

Heather M. Callaway *et al.*

Corresponding author: Erica Ollmann Saphire, erica@lji.org

Sci. Adv. **8**, eabp9151 (2022)
DOI: 10.1126/sciadv.abp9151

The PDF file includes:

Other Supplementary Material for this manuscript includes the following:

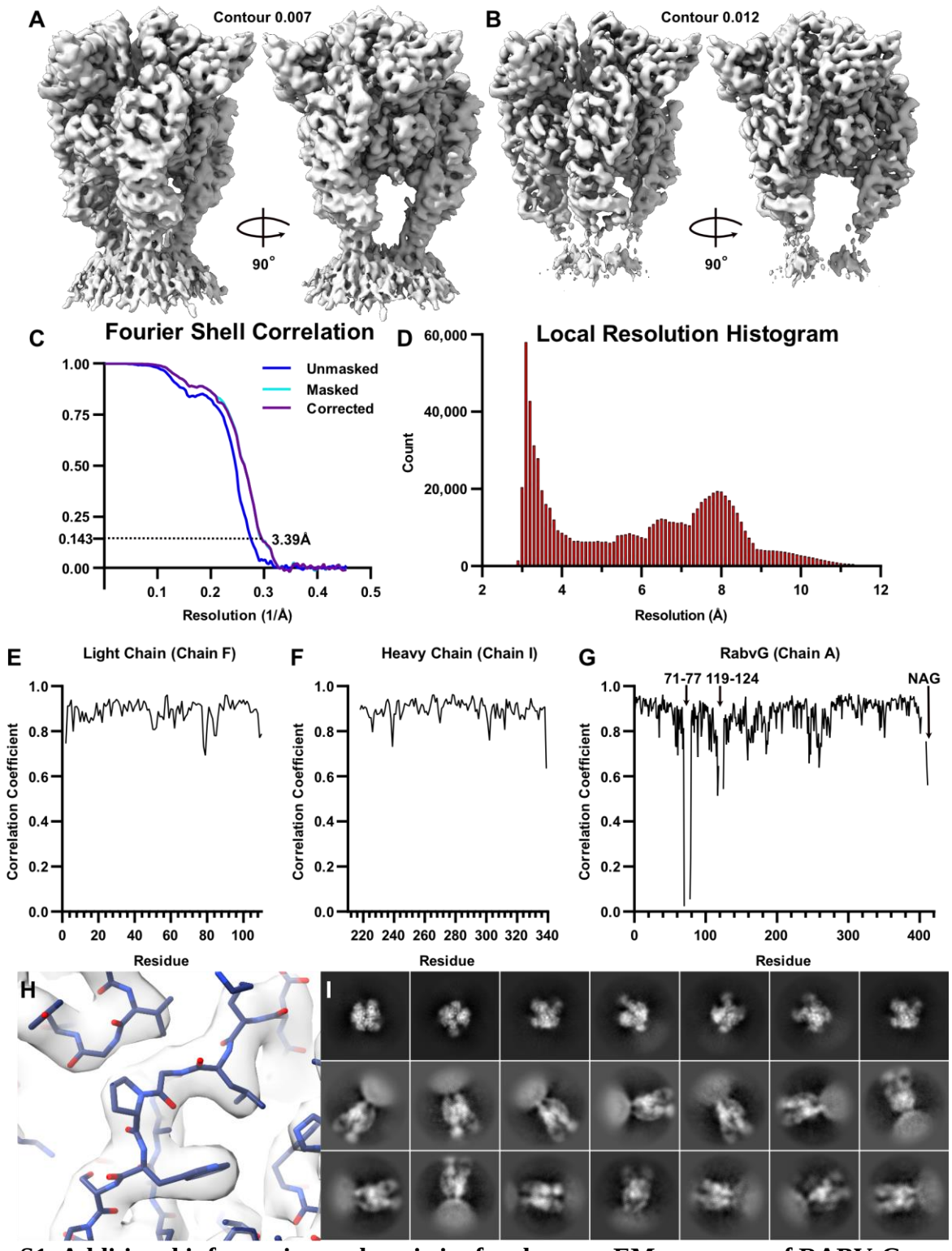

Fig. S1. Additional information and statistics for the cryo-EM structure of RABV-G complexed with neutralizing antibody RVA122. (A-B) Electron density maps at low (A) and high (B) contour levels. **(C)** Fourier Shell correlation curve. **(D)** Local resolution histogram. **(E-G)** Correlation coefficient graphs for the RVA122 light chain (E), RVA122 heavy chain (F), and

RABV-G (G). **(H)** Zoomed map showing the atomic model fit into electron density. **(I)** Representative 2D classes of cryo-EM particles used in 3D reconstruction.

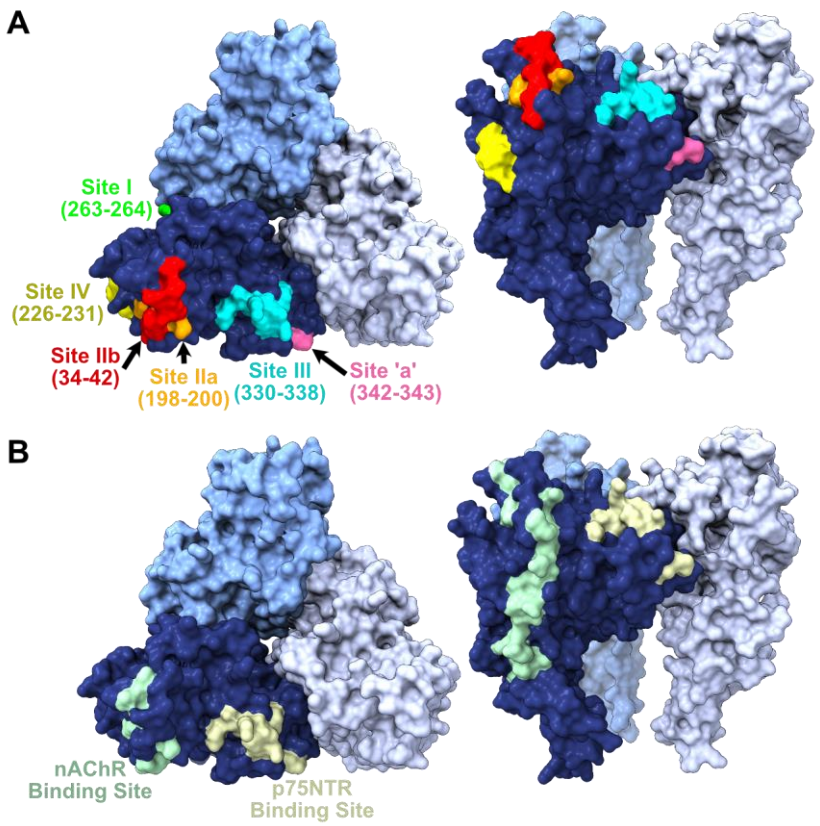

Fig. S2. RABV-G antigenic sites and receptor binding sites. (A) Known RABV-G antigenic sites mapped onto the trimeric RABV-G structure, with residue numbers indicated. **(B)** Approximate receptor binding sites for the nicotinic acetylcholine receptor (nAChR) and the p75 neurotrophin receptor (p75NTR).

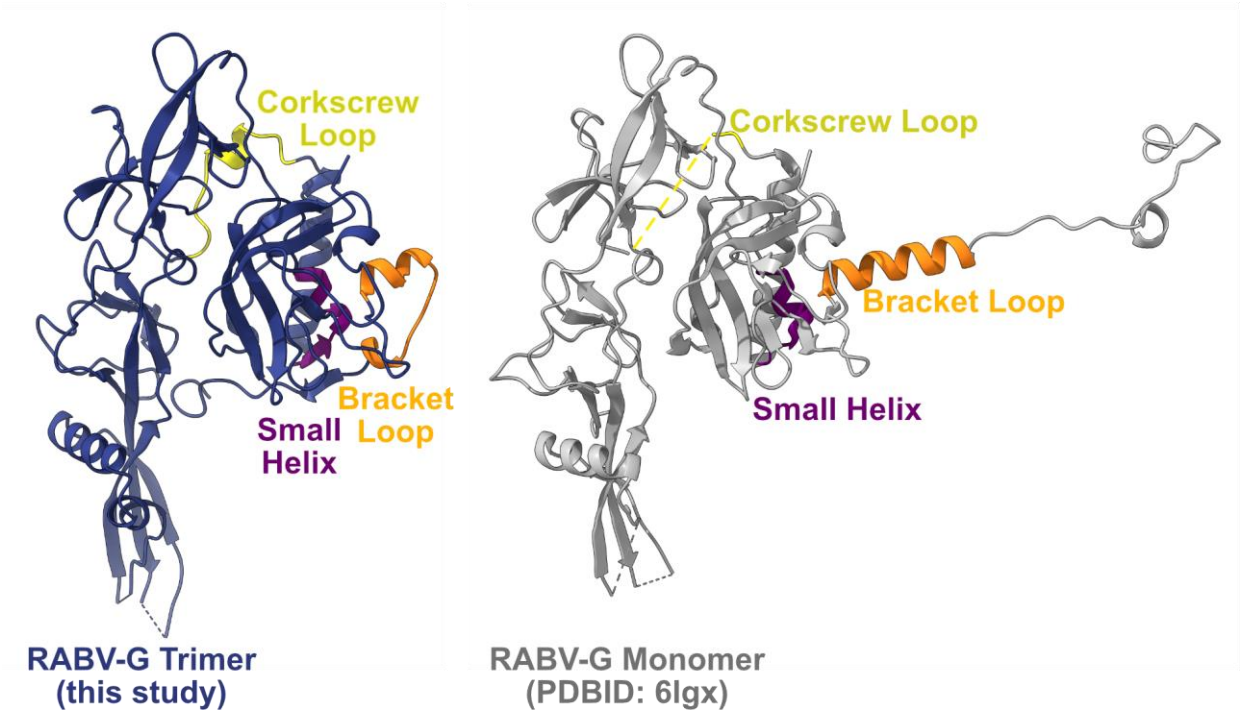

Fig. S3. Pre-fusion RABV-G trimers and alternate pre-fusion RABV-G monomers have different conformations of loops at the trimeric interface. Structure of one RABV-G protomer from this study (left) and a RABV-G monomer from a crystal structure (PDBID: 6lgx) (right), with the small helix (purple), corkscrew loop (yellow), and bracket loop (orange) marked.

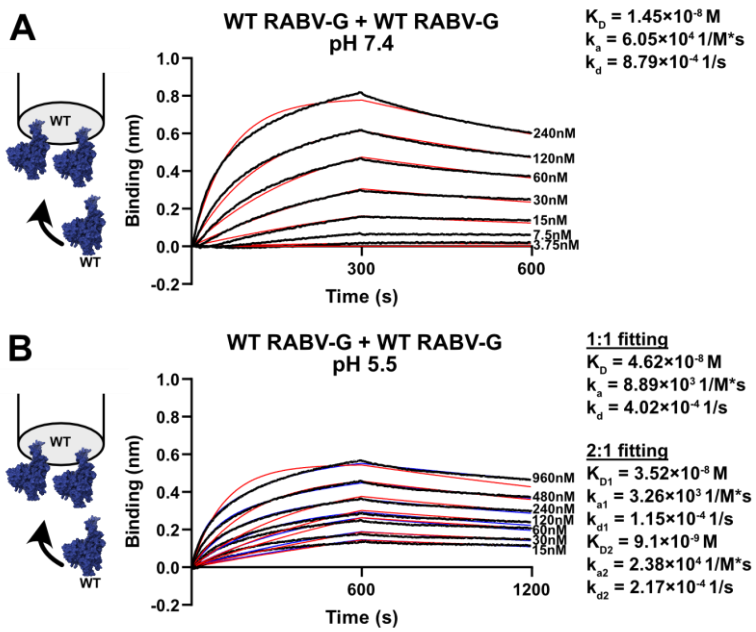

Fig. S4. RABV-G soluble ectodomain binding kinetics. Bio-layer interferometry measurements of RABV-G protomer binding at pH 7.4 **(A)** and pH 5.5 **(B)**. 1:1 curve fitting (red, pH 7.4 and 5.5) and 2:1 curve fitting (blue, pH 5.5 only) are shown. Curves were fitted using the Octet Data Analysis HT software version 11, with global fitting and either a 1:1 fitting model (A) or both 1:1 and 2:1 fitting models (B). Experiments were performed in duplicate.

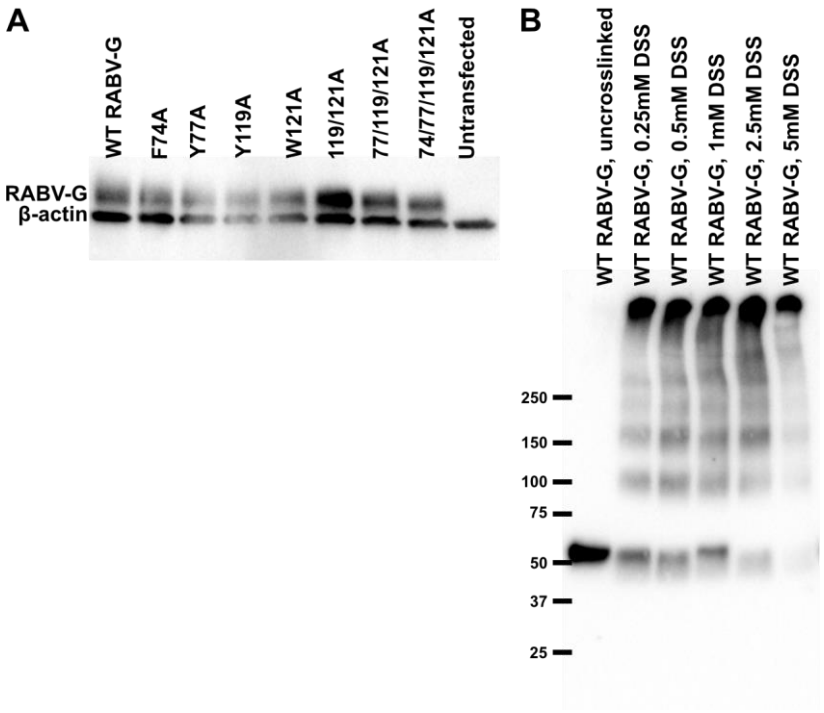

Fig. S5. Expression of RABV-G soluble ectodomains and use of an alternate crosslinker. A) Western blot showing total protein expression levels of RABV-G soluble ectodomains and β-actin (loading control) from lysed cells. **B)** Wild-type RABV-G ectodomains crosslinked with 0.25-5mM DSS.

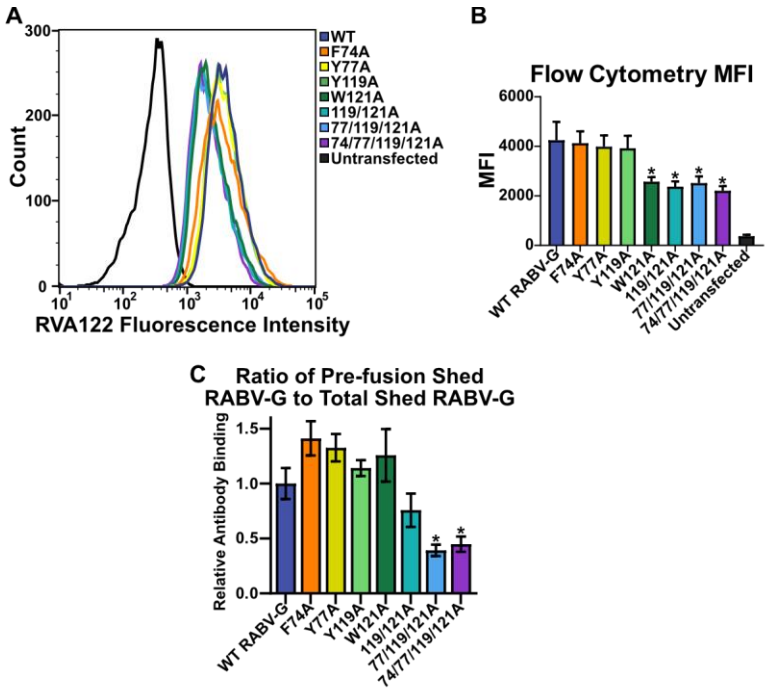

Fig. S6. Fusion loop point mutants affect protein conformation and shedding for full-length RABV-G. (A-B) Flow cytometry quantifying the level of surface-expressed, full-length RABV-G in the pre-fusion conformation. **(C)** Ratio of pre-fusion shed RABV-G to total shed RABV-G in an ELISA quantifying shed RABV-G. Statistical significance of differences were analyzed using ANOVA. Error bars indicate SEM for three biological replicates. * $p<0.05$; ** $p<0.01$.

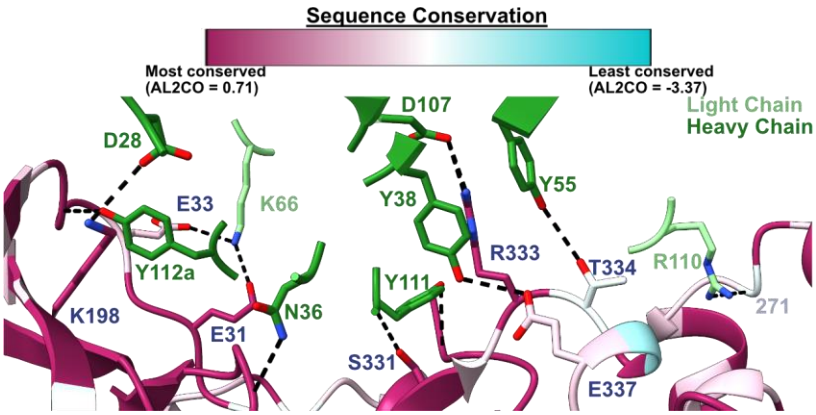

Fig. S7. Sequence conservation among type 1 lyssaviruses at the RVA122 binding site. A sequence alignment was created from European Bat Lyssaviruses 1 (YP_001285391.1) and 2 (YP_001285396.1), Khujand virus (YP_009094330.1), Aravan Lyssavirus (YP_007641395.1), Bokeloh Bat Lyssavirus (YP_009091812.1), Duvenhage virus (NC_020810.1), Irkut virus (AFP74571.1), and PV strain rabies virus (NC_001542.1). ChimeraX 1.2.5 (*39*) was used to color RABV-G residues according to sequence conservation.

A

Reference sequence nucleotide position	Nucleotide substitution	Amino Acid substitution (G gene)	P1	P6	P7
4555	C → A	**P137Q**	<2	78	96.6
5142	C → A	**R333S**	<2	99.9	99.8

B

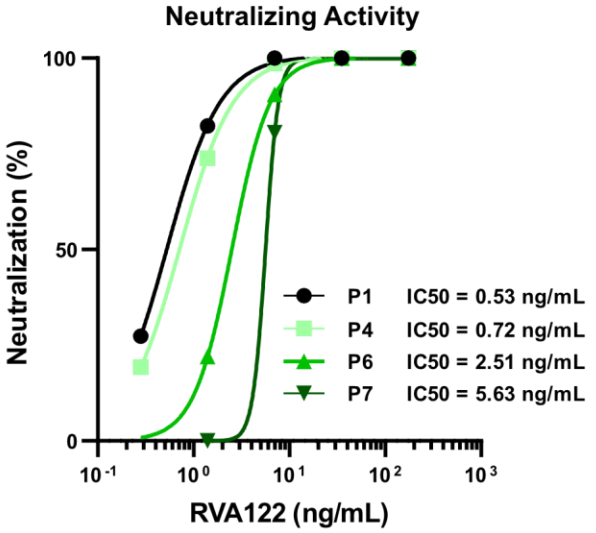

C

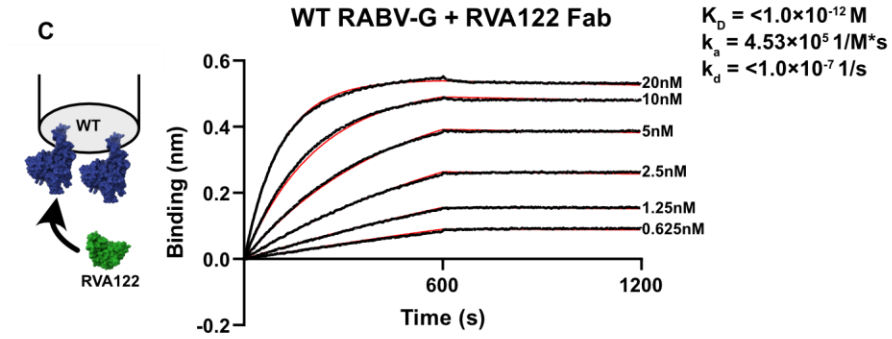

D

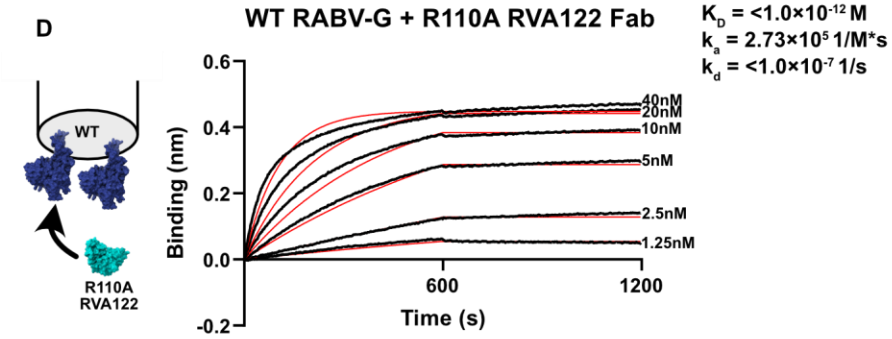

E

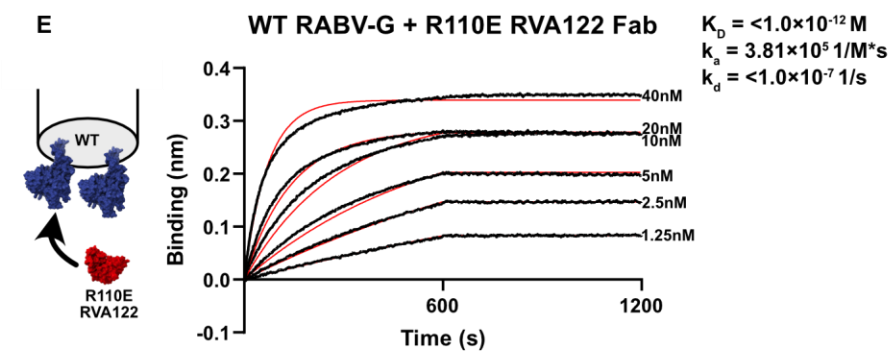

Fig. S8. RABV-G escape mutations and the effect of RVA122 residue R110 on binding. A) NGS sequencing of the escape mutant selected with RVA122. Nucleotide positions are from the Tha-GFP RABV reference sequence (EVAg collection Ref-SKU: 014V-03195). **B)** RVA122 neutralization on sequential passages of Tha-GFP RABV. The IC_{50} concentration for each passage was calculated using GraphPad Prism 9 (non-linear regression, best fit extrapolation). **(C-E)** Bio-layer interferometry measurements of binding kinetics between RABV-G and wild-type RVA122 Fab (C), R110A RVA122 Fab (D), and R110E RVA122 Fab (E). 1:1 curve fitting (red) is shown. Curves were fitted using the Octet Data Analysis HT software version 11, with global fitting and a 1:1 fitting model. Experiments were performed in duplicate.

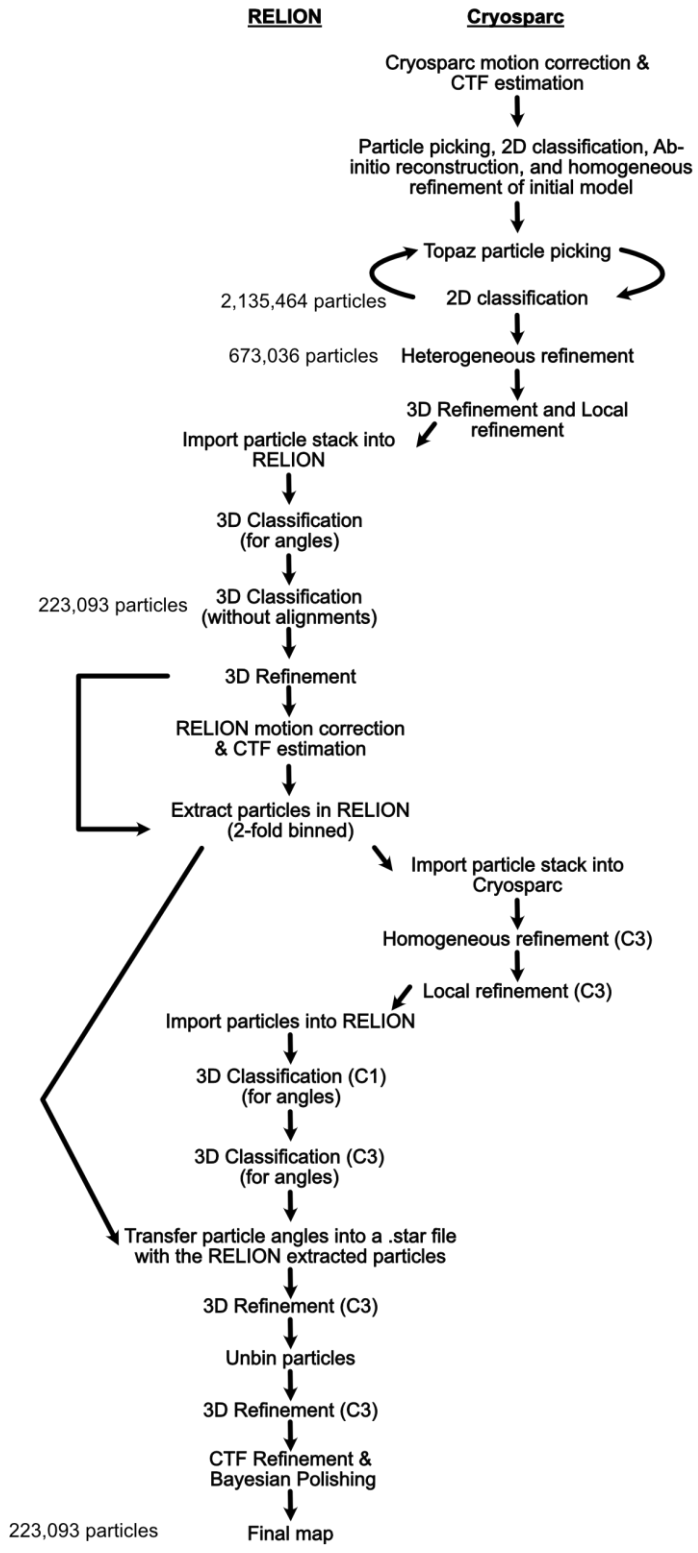

Fig. S9. Supplemental Figure 9. Cryo-EM data processing method for the high-resolution RABV-G/RVA122 complex.

	High Resolution RABV-G/RVA122 Complex	Low Resolution RABV-G/RVA122 Complex		
		3 engaged fusion loops	2 engaged fusion loops	0 engaged fusion loops
Map Statistics				
Movies	6,305	1,969		
Particles	223,092	9,627	32,409	10,144
B-factor	140.5	299.9	256.7	382.7
Resolution (Å)	3.39	7.05	5.71	6.92
Box size (px)	256	256		
Pixel size (Å/px)	1.1	1.15		
Microscope	Titan Krios	Talos Arctica		
Detector	Gatan K3	Gatan K2		
Total dose ($e^-/Å^2$)	50	26.74		
Frames	50	55		
Dose per frame ($e^-/Å^2$)	1	0.49		

Molprobity statistics	
All-atom clashscore	5.16
Ramachandran plot:	
Outliers	0.00%
Allowed	3.11%
Favored	96.89%
Cbeta outliers	0.00%
Rotamer outliers	0.00%
Peptide plane:	
Cis-proline	0.00%
Cis-general	0.00%
Twisted proline	0.00%
Twisted general	0.00%

Table S1. CryoEM map and model statistics.

Movie S1. 3D variability analysis of RABV-G fusion loops.